INTERNATIONAL JOURNAL OF HYDROGEN ENERGY 47 (2022) 29441–29455

Available online at www.sciencedirect.com

ScienceDirect

journal homepage: www.elsevier.com/locate/he

Performance and durability of Ni–Co alloy cermet anodes for solid oxide fuel cells

Kohei Matsumoto [a], Yuya Tachikawa [a,b,c], Stephen M. Lyth [b], Junko Matsuda [b,c], Kazunari Sasaki [a,b,c,d,*]

[a] Department of Hydrogen Energy Systems, Faculty of Engineering, Kyushu University, Motooka 744, Nishi-ku Fukuoka 819-0395, Japan

[b] International Research Center for Hydrogen Energy, Kyushu University, Motooka 744, Nishi-ku Fukuoka 819-0395, Japan

[c] Next-Generation Fuel Cell Research Center (NEXT-FC), Kyushu University, Motooka 744, Nishi-ku Fukuoka 819-0395, Japan

[d] Platform of Inter-/Transdisciplinary Energy Research (Q-PIT), Kyushu University, Motooka 744, Nishi-ku Fukuoka 819-0395, Japan

HIGHLIGHTS

- Ni–Co alloy cermet anodes for solid oxide fuel cells were developed.
- Durability up to 50 redox cycles was improved by alloying Ni with Co.
- 1000-h durability using highly-humidified hydrogen fuel was verified.
- Ni–Co alloy is a robust anode material even in 80%-humidified hydrogen fuels.

ARTICLE INFO

Article history:
Received 23 April 2022
Received in revised form
18 June 2022
Accepted 26 June 2022
Available online 18 August 2022

Keywords:
Solid oxide fuel cell
Anode
Ni–Co alloy
Redox tolerance
Robustness

ABSTRACT

Ni alloys are examined as redox-resistant alternatives to pure Ni for solid oxide fuel cell (SOFC) anodes. Among the various candidate alloys, Ni–Co alloys are selected due to their thermochemical stability in the SOFC anode environment. Ni–Co alloy cermet anodes are prepared by ammonia co-precipitation, and their electrochemical performance and microstructure are evaluated. Ni–Co alloy anodes exhibit high durability against redox cycling, whilst the current-voltage characteristics are comparable to those of pure Ni cermet anodes. Microstructural observation reveals that cobalt-rich oxide layers on the outer surface of the Ni–Co alloy particles protect against further oxidation within the Ni alloy. In long-term durability tests using highly humidified hydrogen gas, the use of a Ni–Co cermet with Gd-doped CeO_2 suppresses degradation of the power generation performance. It is concluded that Ni–Co alloy cermet anodes are highly attractive for the development of robust SOFCs.

* *Corresponding author*. Kyushu University, Next-Generation Fuel Cell Research Center, Motooka 744, Nishi-ku Fukuoka 819-0395, Japan.
E-mail address: sasaki@mech.kyushu-u.ac.jp (K. Sasaki).

https://doi.org/10.1016/j.ijhydene.2022.06.268

Introduction

Fuel cells are electrochemical devices that efficiently convert the chemical energy of fuel and an oxidant into electricity. Specifically, SOFCs have advantages such as high efficiency for power generation and fuel flexibility, without the requirement for precious metal catalysts due to their high operating temperature (e.g. from 600 to 900 °C) [1–6]. Stationary combined heat-and-power fuel cell systems have already been commercialized. For example, the number of residential fuel cell systems (commonly called "ENE-FARM") installed in Japan has already exceeded 400,000 as of August 2021 [7]. The polymer electrolyte fuel cell class of ENE-FARM was launched in 2009, followed by the SOFC class in 2011, and the percentage of the SOFC class is gradually increasing largely due to its higher efficiency [8]. In addition, a 250 kW class SOFC-micro gas turbine hybrid system has been commercialized by Mitsubishi-Hitachi Power Systems (now Mitsubishi Heavy Industries), with a 1 MW system in the planning stage [9]. Meanwhile, Ceres Power in UK has set a target of producing SOFC systems with a cumulative capacity of several hundred MW, having signed commercial contracts with Robert Bosch in Germany, and Doosan in Korea [10]. Moreover, Bloom Energy in the U.S. sold a cumulative 80.9 MW of SOFC system capacity by 2018, representing a leading effort in the commercialization of SOFC systems [11]. However, research and development into SOFCs that operate, e.g., at relatively lower temperatures are still in progress due to the limited availability of materials which can maintain their performance for long periods of time at elevated temperature [12,13].

Nickel cermets are widely used as SOFC anodes, and are comprised of Ni and an electrolyte component such as yttria-stabilized zirconia (YSZ) [1–6,14]. However, the Ni-based electronic conducting network in these anodes can be disrupted by repeated cycling of redox reactions, associated with the coarsening and aggregation of Ni particles [15]. Such redox processes occur when the fuel supply is interrupted upon system startup and shutdown, resulting in the deterioration of the overall efficiency of SOFC systems [16–26]. The development of SOFC anodes with high redox cycle durability has another important practical benefit, eliminating the need for an inert gas supply to prevent Ni oxidation during system shutdown, significantly simplifying system design and control.

Therefore, it is desirable to develop SOFC anodes with high durability and resilience against redox cycling for the more widespread use of SOFCs. To solve this issue, the use of more redox stable materials such as strontium titanate ($SrTiO_3$) may be helpful [27–30], whilst it can be doped with a higher valence cation at the A site to improve its electronic conductivity [31–35]. Strontium titanate doped with La^{3+} at the A site (i.e, $Sr_{0.9}La_{0.1}TiO_3$, commonly known as LST) exhibits high electronic conductivity under SOFC operating conditions [31]. Furthermore, LST has a comparable thermal expansion coefficient to that of zirconia-based electrolyte materials [32]. Futamura et al. demonstrated that, impregnation of porous anodes with fine metallic catalyst nanoparticles such as Ni and Rh, high durability against redox cycling could be achieved when supplied with 3% humidified hydrogen fuel, without sacrificing electrochemical performance [30]. However, when hydrogen-related fuel gas is supplied to SOFC systems, the water vapor concentration is reported to increase near the fuel gas outlet, and thus the Ni anode catalysts tend to oxidize [21], one of the major degradation mechanisms of SOFC anode materials. The electrochemical performance of impregnated anodes at high fuel utilization (i.e. at a higher water vapor concentration in the fuel feed) is slightly lower than that of conventional anodes [29,30]. For successful commercialization, both high performance and durability must be achieved simultaneously. The stability of anodes at high fuel utilization, if improved, enables higher power generation efficiency, because a larger fraction of the fuel can be utilized for power generation.

As an alternative approach, novel SOFC anodes are being developed using Ni alloyed with transition metal elements rather than using pure Ni. In general, metallic Ni-alloys can exhibit higher electronic conductivity compared to ceramics such as donor-doped $SrTiO_3$. When such alloy-based cermet anodes are exposed to an oxidizing atmosphere, the formation of a surface oxide layer suppresses further oxidation within the alloy particles, and it is possible that this could improve the durability against redox cycling in SOFCs. However, it is well known that doped elements in alloys generally act as scattering sites detrimental to electronic conductivity [36]. Therefore, it is important that Ni-alloys should exhibit both sufficient electronic conductivity and catalytic activity for efficient SOFC operation, even under a hydrogen-based fuel supply. Araki et al. already reported the synthesis of various Ni alloy anodes using a spray drying technique, and investigated the effect of alloying on SOFC efficiency and H_2S poisoning [37]. Meanwhile, Ishibashi et al. prepared NiO-containing complex oxide powders and various Ni alloy anodes by ammonia co-precipitation, and reported electrochemical performance and redox cycling durability, finding that cobalt is a promising element for the formation of surface oxide layers for enhanced durability against redox cycling [38].

Although the durability may be improved using alloying, cobalt is classed as a critical raw material, i.e. an element of high economic importance, but limited supply [39]. The price of Co will continue to increase due to the rise in demand for lithium-ion batteries, especially in battery electric vehicles (BEVs) [39–41]. As such, the overall amount of cobalt in SOFCs should be minimized where possible, so that the redox durability can be enhanced without risking supply chains or increasing the cost. The source of cobalt and the related geopolitical situation should also be considered.

The objective of this study is to develop highly durable Ni–Co alloy cermet anodes, whilst keeping the Co content as low as possible. Gadolinium-doped ceria (GDC) is selected as the electrolyte component in the anodes, and the effect of systematically adjusting the Ni:Co ratio on SOFC performance and microstructure will be investigated. Long-term tests will also be conducted at high fuel utilization (i.e. using a highly-humidified hydrogen supply).

Experimental procedures

Thermochemical equilibrium calculations

A stability diagram was computationally obtained using the software FactSage (Version 7.4, Thermfact Ltd., Canada) in order to examine the thermochemically stable phases of Ni–Co alloys in reducing and oxidizing atmospheres at 800 °C (a typical SOFC operating temperature). In this study, we used the Phase Diagram module of FactSage to derive the Ni–Co and NiO–CoO phase diagrams and the Ni/NiO and Co/CoO phase boundaries.

Cell fabrication

NiO and CoO composite oxide powders were prepared by ammonia co-precipitation, as described in Fig. 1. $Ni(NO_3)_2 \cdot 6H_2O$ and $Co(NO_3)_2 \cdot 6H_2O$ (Kishida Chemical Co., Ltd., Japan) were used as the precursors for co-precipitation. Briefly, ammonia solution was added dropwise to an aqueous solution containing Ni and Co ions (in various ratios) to simultaneously precipitate these complex hydroxides [38]. The precipitates were then filtered, dried at 100 °C for 10 h in air, and calcined at 1000 °C for 2 h in air. The resulting composite oxide powders were mixed with GDC ($Ce_{0.9}Gd_{0.1}O_2$, Rhodia, ULSA grade, USA) in a mass ratio of 48.1:51.9, resulting in a volume ratio of 50:50 for pure NiO (slightly changing when CoO was also incorporated). Ni–Co-GDC cermet anodes were prepared with a variety of molar ratios, Ni:Co = (100-x):x, where x = 0, 5, 10, 20, and 30, herein referred to as $Ni_{(100-x)}Co_x$-GDC. Lanthanum strontium manganite (LSM, $(La_{0.8}Sr_{0.2})_{0.98}MnO_3$, Praxair, USA) and scandium-stabilized zirconia (ScSZ, Daiichi Kigenso Kagaku Kogyo Co., Ltd., Japan) were used in the cathode. At the cathode side, a 1:1 LSM:ScSZ mass ratio was used close to the electrolyte, and 100% LSM powder was used close to the current collector [15,38].

Fig. 2 shows a schematic of the cell structure. In this study, the classical electrolyte-supported structure rather than electrode-supported or metal-supported structures is selected, in order to extract the anode-side voltage losses using a reference electrode [38]. The solid electrolyte is comprised of a plate of ScSZ (10 mol% Sc_2O_3, 1 mol% CeO_2, 89 mol% ZrO_2) with a diameter of 20 mm and a thickness of 200 μm. The anode layer was screen-printed onto the ScSZ electrolyte followed by heat-treatment at 1300 °C for 3 h in air. The cathode layer was then screen-printed onto the opposite side of the electrolyte followed by heat-treatment at 1200 °C for 5 h in air. The anode and cathode layers were both approximately 40 μm in thickness after heat-treatment. To separate the anode and cathode overvoltages, a reference electrode with an area of ca. 4 mm^2 size was placed 2 mm away from the cathode, using Pt paste. A Pt mesh was attached to the surface of each electrode as a current collector, set on the electrodes after screen printing, and then each electrode was heat-treated. The electrode area was 8 × 8 mm^2 (0.64 cm^2).

Cell performance test

Fig. 3 shows the configuration of the electrochemical experimental setup. Cell performance tests were conducted using automated fuel cell evaluation systems (AutoSOFC, TOYO Corporation, Japan). Before measuring the cell polarization curves, the cell was sealed using a Pyrex glass ring and increasing the temperature to 1000 °C at 200 °C h^{-1}. Then, the cell temperature was maintained at 1000 °C, and 3% humidified hydrogen was supplied at 100 mL min^{-1} for 1 h to reduce the metal oxide in the anode to the metallic state. The selected reduction temperature (1000 °C) is sufficient to reduce NiO to metallic Ni in the thin porous anode layers of the electrolyte-supported cells [15,21,29,30,38], whereas a higher temperature may be required for e.g. anode-supported and metal-supported cells with thicker anode layers. The current-voltage (I–V) characteristics were then measured at 800 °C with 3% humidified hydrogen fuel supplied to the anode. The anode voltage (potential) was measured relative to the reference electrode on the cathode

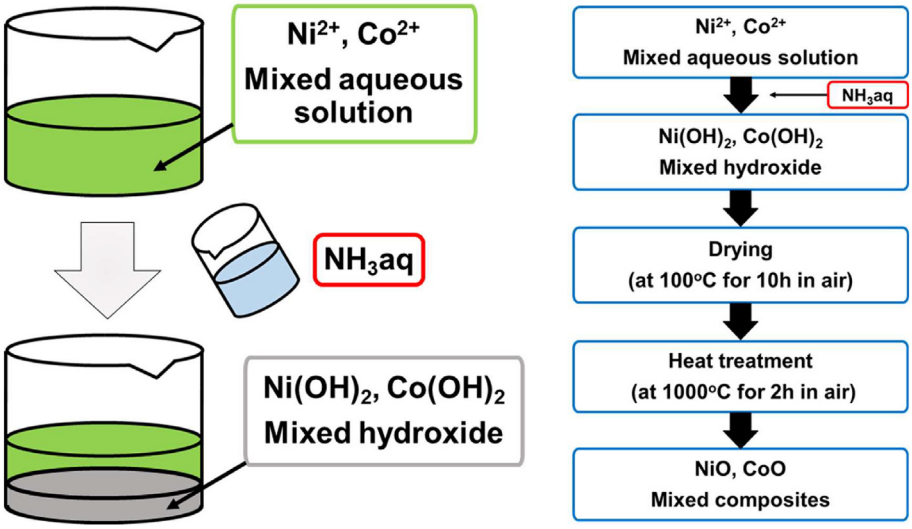

Fig. 1 – Method used in this study for the synthesis of mixed NiO and CoO composite powders by ammonia co-precipitation.

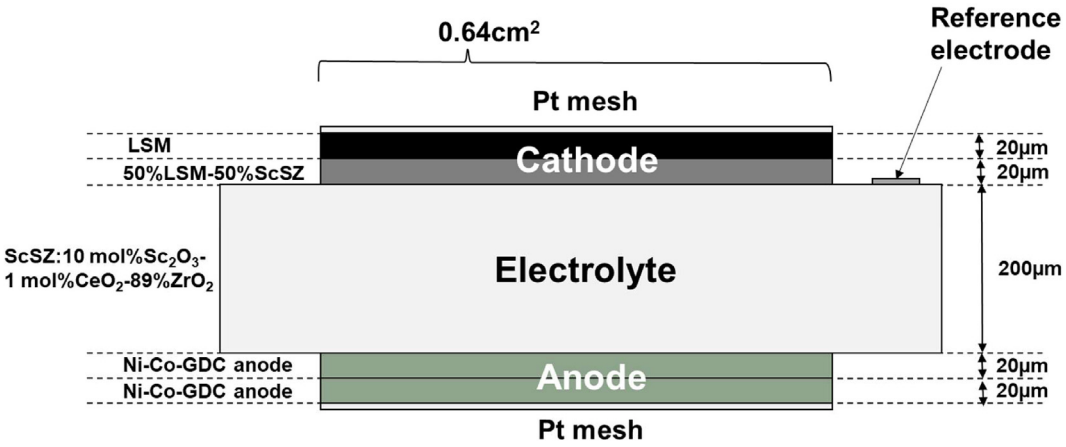

Fig. 2 – Schematic of the SOFC single cell used in this study.

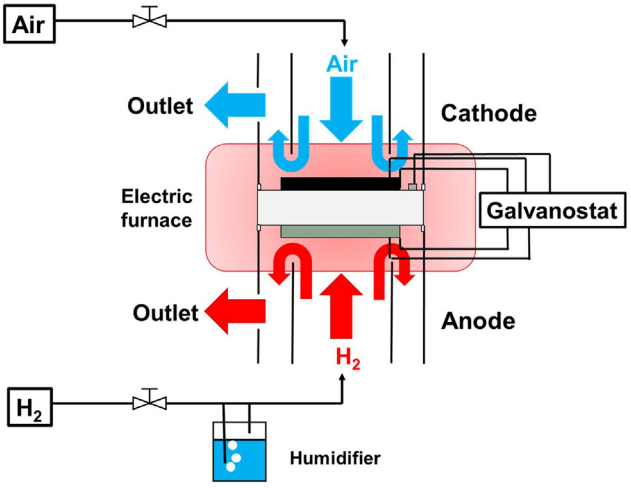

Fig. 3 – Schematic of the experimental setup for the electrochemical measurements.

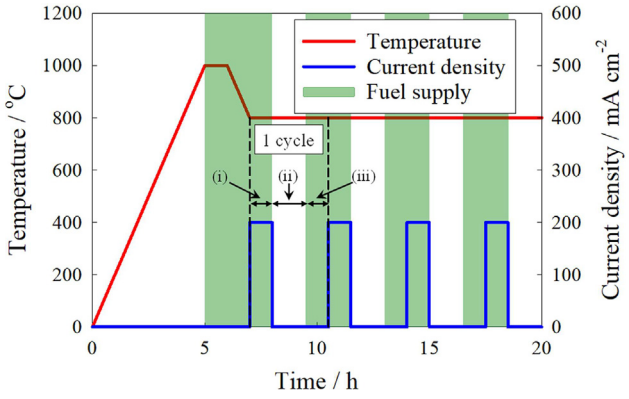

Fig. 4 – Redox cycling test protocol for redox tolerance evaluation [15], consisting of three phases: (i) with current and fuel supply, (ii) without current and fuel supply, and (iii) with fuel supply but without current.

side. As the anode voltage includes both ohmic and non-ohmic overvoltages, these overvoltages (i.e., anode-side ohmic loss and anodic overvoltage) were separated via the current interrupt method [15,38]. Each electrochemical measurement was repeated three times, and the average values and their standard deviation are given to check their uncertainty.

Redox cycling test

Redox cycling tests were conducted at 800 °C to evaluate the durability of the anodes, as described in Fig. 4 [15]. First, the cell was operated for 1 h at a current density of 0.2 A cm^{-2} with 3% humidified hydrogen fuel supply (i); then, the fuel supply was interrupted for 1.5 h (ii); and finally, the supply of 3% humidified hydrogen was restarted (iii). These three steps are regarded as one cycle, and 50 cycles were applied in total. The anode voltage, non-ohmic anodic overvoltage, and anode-side ohmic loss were measured during these cycling tests.

High fuel utilization test

The I–V characteristics and durability were also evaluated during continuous power generation up to 1000 h under 80% humidified hydrogen supply. The I–V characteristics were measured under the same conditions as the cell performance test section described above. The anode voltage, anodic overvoltage, and anode-side ohmic loss were measured at a current density of 0.2 A cm^{-2} and 80% humidified hydrogen over a course of 1000 h.

Microstructural observation

Scanning electron microscopy (SEM) with energy-dispersive X-ray spectroscopy (EDS) was performed to evaluate the distribution of elements in the whole of anodes using dual-beam SEM (Versa 3D, FEI, USA). High-resolution observation and elemental analysis on the $Ni_{(100-x)}Co_x$-GDC anodes were carried out by means of scanning transmission electron microscopy (STEM, JEM-ARM200F, JEOL, Ltd., Japan).

Results and discussion

Phase diagrams

Phase diagrams of Ni–Co and NiO–CoO systems were calculated to estimate the stable phases in both reducing and oxidizing atmospheres. The resulting phase diagrams are shown in Fig. 5, where the triangular symbols specify the positions at 800 °C for the following compositions: Ni-GDC (black); $Ni_{95}Co_5$-GDC (red); $Ni_{90}Co_{10}$-GDC (green); $Ni_{80}Co_{20}$-GDC (blue); and $Ni_{70}Co_{30}$-GDC (pink).

Fig. 5(a) predicts that all five compositions will form Ni–Co alloys with fcc structure in reducing atmosphere. Fig. 5(b) predicts that all five compositions will form a solid solution with a single-phase NiO crystal structure in oxidizing atmosphere. Therefore, in the reducing atmosphere of the SOFC anode, the material is expected to be a true alloy, with Co dissolved in the Ni lattice. Fig. 6 shows a stability diagram calculated after Ishibashi et al. [38], in which the coexisting equilibrium oxygen partial pressures of the metallic and oxide states of Ni and Co are plotted as a function of temperature. In this figure, the equilibrium boundary between Co and CoO is located at a lower oxygen partial pressure compared to Ni/NiO. This indicates that Co is slightly more easily oxidized compared to Ni. As such, when the fuel supply is interrupted in SOFC anodes, Co will be oxidized first, forming an oxide surface layer on the Ni–Co alloy. Evidence of the formation of a Co-rich layer on surface of the Ni–Co alloy has already been observed via higher-resolution TEM [38]. Therefore, based on the calculated thermochemical stability of Ni–Co alloys in reducing and oxidizing atmospheres, it is expected that the redox cycle durability could be improved by alloying Ni with Co through the formation of a protective surface oxide layer. Further analysis is of scientific and technological interest, such as in-situ microstructural observation of redox processes at Ni–Co alloy surfaces.

Fig. 5 also confirms that a solid solution will be formed at elevated temperature in both the Ni–Co and NiO–CoO systems. Whilst the sintering temperature of the anodes was around 1300 °C, which is relatively low compared to typical anode-supported cells, these phase diagrams predict the formation of complete solid solutions even at higher sintering temperatures above 1300 °C.

I–V characteristics

Fig. 7 shows representative plots of (a) the anode voltage (anode potential) relative to the reference electrode, (b) the anodic overvoltage, and (c) the anode-side ohmic losses for each anode material, with error bars indicating their standard deviation, measured at 800 °C. Fig. 7(a) reveals that the pure Ni-GDC anode exhibits the highest I–V performance. As shown in Fig. 7(b) and (c), the non-ohmic anodic overvoltage and the ohmic losses of anodes for which $x = 10$, 20, and 30 are higher than those of the pure Ni-GDC anode. These results suggest that Ni is more active than Co, and that alloying Ni with Co leads to a decrease in electronic conductivity. The dependence of overvoltage on the Co concentration above 10% will be a matter for future studies.

In contrast, the anode for which $x = 5$ exhibits similar I–V characteristics as the pure Ni-GDC anode, as shown in Fig. 7(a). This result indicates that the decrease in power generation performance due to the addition of Co is negligible when the content of Co is sufficiently low. This result suggests that, by optimizing the ratio of Ni and Co, it is possible to prepare alloy-based cermet anodes with high redox cycle durability while maintaining power generation performance.

Redox stability

Following the protocol outlined in Fig. 4, the durability against redox cycling was measured three times for each of the five anode compositions. Typical results for the change in (a) anode voltage; (b) anodic overvoltage; and (c) anode-side ohmic loss during the test, measured at 800 °C, are shown in Fig. 8. The percentage of anode voltage drop from the first cycle to the 50th cycle is shown in Fig. 9, with error bars based on the standard deviation calculated from the results of three cells for each composition.

In Fig. 8, the observed changes during the early stages of the tests could be caused by e.g. the thermal history of the cells during the sintering processes. Regarding durability, Fig. 8(a) reveals that the anode voltage for pure Ni-GDC significantly drops over 50 redox cycles, finally reaching around 0.7 V. In contrast, all the Ni–Co alloy anodes display a much smaller drop in anode voltage, dropping to ca. 0.87 V after 50 redox cycles. Fig. 9 plots the percentage change in anode voltage after 50 cycles, and a clear trend of decreasing degradation with increased Co content emerges. The largest difference is observed between the pure Ni-GDC anode and the $Ni_{95}Co_5$-GDC anode, indicating that the addition of even a small amount (5%) of Co can considerably improves the durability against redox cycling.

Fig. 8(b) and (c) reveal that the addition of Co suppresses increases in both the non-ohmic anodic overvoltage and the ohmic losses during redox cycling. This is attributed to the preferential formation of a Co-based surface oxide layer on the Ni–Co alloy, helping to suppress redox-induced aggregation of Ni particles, and thus preventing a decrease in electrode reaction area and maintaining electron-conducting network.

Based on the fact that the durability of SOFC against redox cycling can be significantly improved even with the addition of just 5 mol% Co, herein the $Ni_{95}Co_5$-GDC anode is selected as a suitable anode composition for combining durability with minimal content of critical raw materials. Therefore, in the next section, the performance and durability of SOFCs with pure Ni-GDC and $Ni_{95}Co_5$-GDC anodes with 80% humidified hydrogen are evaluated.

I–V characteristics and stability at high fuel utilization

The electrochemical performance and long-term durability of the pure Ni-GDC and $Ni_{95}Co_5$-GDC anodes are herein investigated under more severe operating conditions, namely at higher water vapor partial pressure, simulating higher fuel utilization. The I–V characteristics and durability up to 1000 h were measured at 800 °C using 80% humidified hydrogen supply. Fig. 10(a) compares the initial anode voltage, whilst (b)

and (c) compare the initial anodic overvoltage, and the initial anode-side ohmic loss, respectively. Meanwhile, Fig. 11 shows (a) the anode voltage, (b) the anodic overvoltage, and (c) the anode-side ohmic loss throughout the 1000-h durability test.

Fig. 10 confirms that the Ni-GDC and $Ni_{95}Co_5$-GDC anodes exhibit almost the same I–V characteristics under 80%-humidified hydrogen supply, with the anodic overvoltage and the anode-side ohmic loss also being very similar. This

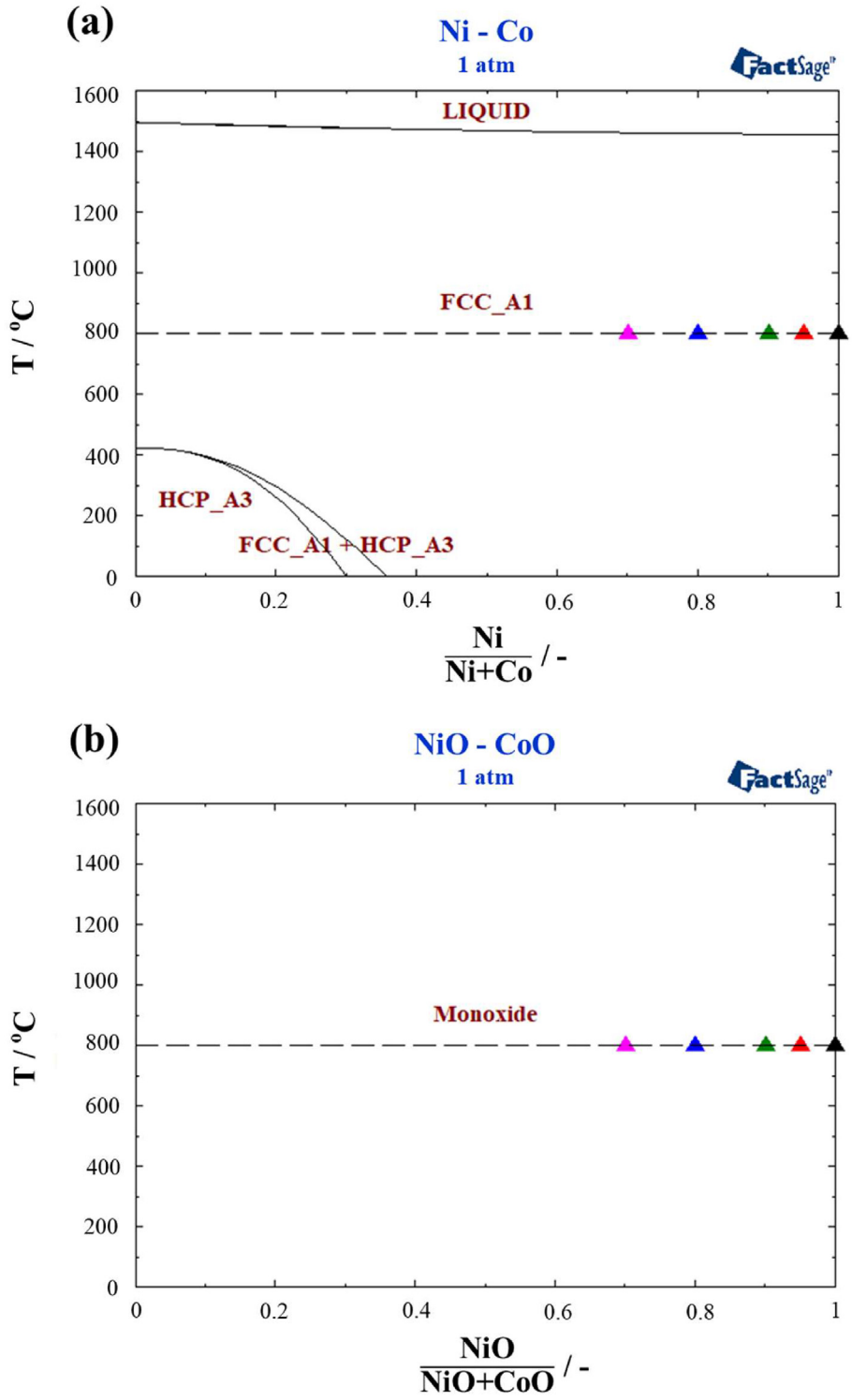

Fig. 5 – Phase diagrams of: (a) the Ni–Co system, and (b) the NiO–CoO system. A1 corresponds to the face centered cubic (fcc) Ni-type structure, and A3 corresponds to the hexagonal close-packed (hcp) Co-type structure at temperatures below 420 °C. The triangular symbols correspond to: Ni-GDC (black); $Ni_{95}Co_5$-GDC (red); $Ni_{90}Co_{10}$-GDC (green); $Ni_{80}Co_{20}$-GDC (blue); and $Ni_{70}Co_{30}$-GDC (pink).

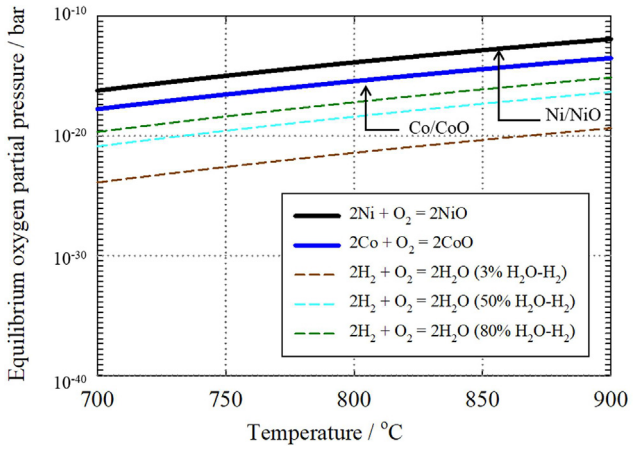

Fig. 6 – Stability diagram of Ni and Co between 700 and 900 °C. The co-existence P(O_2) boundaries of these metals and their oxides are shown as a function of temperature. The equilibrium oxygen partial pressure of the H_2–H_2O system is also shown simulating humidified H_2-based fuel gasses.

confirms that the addition of a low concentration of Co has negligible or slightly positive effect on the I–V performance even at high fuel utilization, simulating the conditions at the downstream of the fuel supply in fuel cell systems, where redox-related degradation tends to occur. The reactions responsible for the slight improvement in electrochemical performance via alloying Ni with Co under these highly-humidified conditions are of scientific interest, where e.g. dealloying, segregation of secondary phases, formation of nano-composites, and/or their co-catalyst effects could occur.

The anode voltage measured over the 1000-h durability test at 800 °C is shown in Fig. 11(a). As the anode voltage in (a) remained stable during 1000 h, certain noisy fluctuation in the raw data shown in (b) and (c) may not influence the overall durability. Fig. 11(a) confirms that the addition of Co slightly improves the long-term durability under highly humidified hydrogen supply. Fig. 11(b) and (c) confirm that this improvement in the long-term durability is mainly associated with a decrease in non-ohmic anodic overvoltage, which is suppressed by the addition of Co.

The non-ohmic overvoltages were averaged, and their standard deviations derived in every 100 h throughout the test, giving 80.2 ± 6.1 mV for the pure Ni-GDC anode, and 44.7 ± 2.0 mV for the $Ni_{95}Co_5$-GDC anode. Matsui et al. previously reported that the Ni surface can be oxidized under highly humidified hydrogen supply, reducing the extent of the triple-phase boundary [42], increasing the non-ohmic overvoltage. As such, it is concluded that the addition of Co does not accelerate this process, and therefore can be used in SOFC anodes even in highly-humidified fuel streams.

Microstructural analysis

To elucidate the reasons for changes in the performance and durability, the distribution and chemical state of Ni and Co in the Ni–Co alloy anodes were measured before the durability test. Fig. 12 shows representative elemental distribution maps

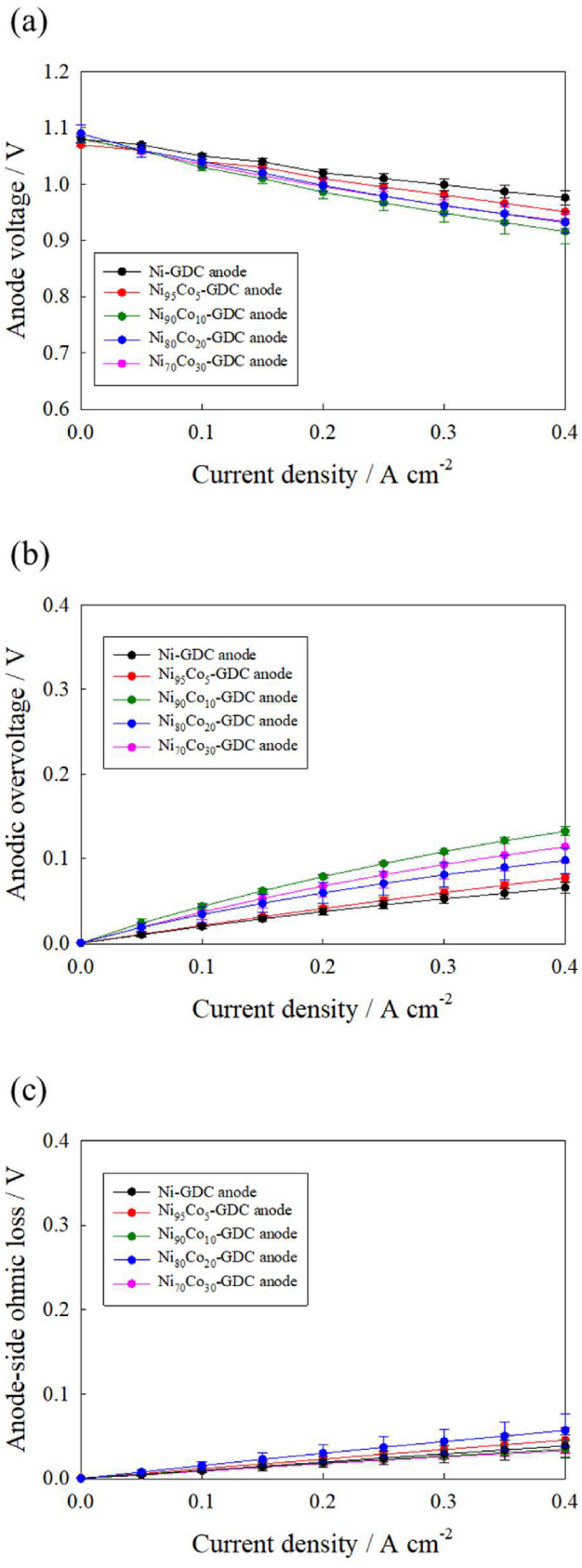

Fig. 7 – Electrochemical performance of single cells, using $Ni_{(100-x)}Co_x$-GDC anodes (x = 0, 5,10, 20 and 30), measured for 3% humidified H_2 fuel: (a) anode voltage, (b) anodic overvoltage, and (c) anode-side ohmic loss.

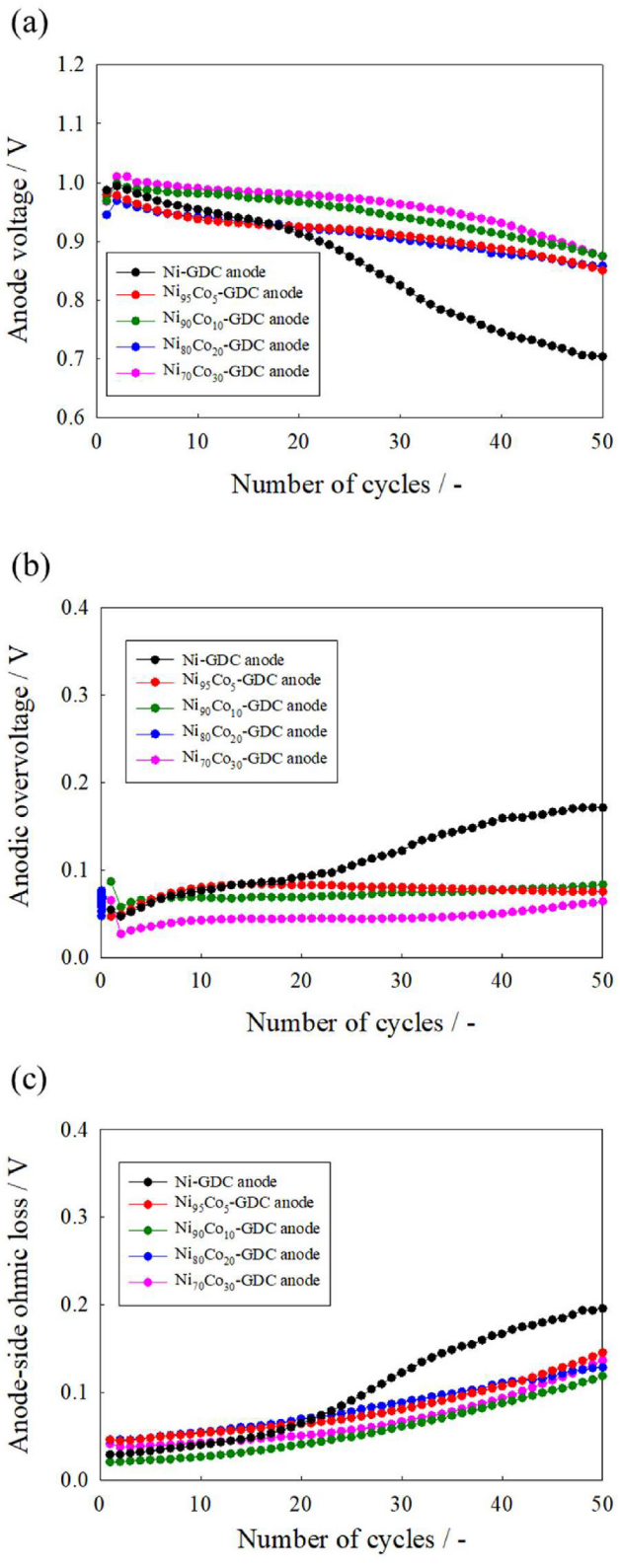

Fig. 8 – Redox cycle durability of single cells, measured for 3% humidified H_2 fuel, using the $Ni_{(100-x)}Co_x$-GDC anodes (where x = 0, 5,10, 20 and 30): (a) anode voltage, (b) anodic overvoltage, and (c) anode-side ohmic loss.

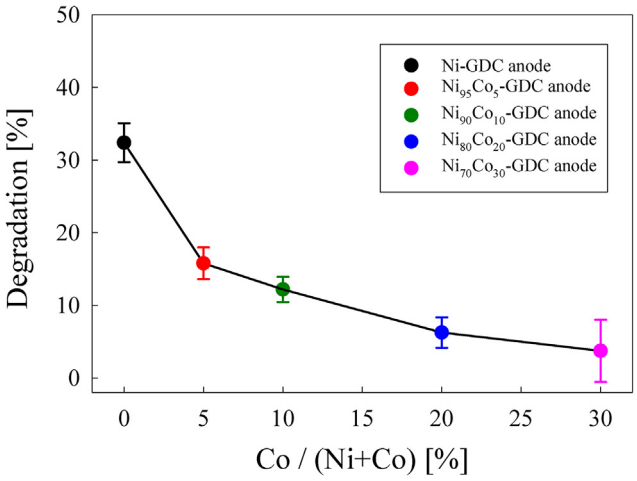

Fig. 9 – Percentage change in anode voltage by the redox cycle tests as a function of Co content, indicating improved voltage retention at higher Co content.

of the $Ni_{95}Co_5$-GDC and $Ni_{70}Co_{30}$-GDC anodes, analyzed by SEM-EDS. As shown in Fig. 12, in both samples (a) and (b), the location of Ni and Co within the anode layers is exactly the same. This analysis confirms that the elemental distributions of Ni and Co are almost identical in both anodes. The molar ratios of Ni and Co obtained by point analysis compiled in Table 1 are very close to the nominal ratios targeted in the co-precipitation synthesis step, namely Ni:Co = 95:5, and Ni:Co = 70:30, confirming the validity of the phase diagram shown in Fig. 5(a).

Fig. 13 shows STEM-EDS elemental distribution maps of the Ni-GDC anode before and after the redox cycling test, for Ni, O and Ce. Before the test, the elemental O distribution largely overlaps with Ce, but not with Ni, suggesting that pure Ni mainly exists as a metal. In contrast, after the durability test, oxygen is observed to additionally be present at the surface of the Ni particles, confirming that nickel particles are oxidized during the durability tests.

Meanwhile, Fig. 14 shows elemental distribution maps for the $Ni_{95}Co_5$-GDC anode before and after the redox cycling test, in this case also including the Co distribution. Before the test, the distributions of Ni and Co closely overlap, and the distributions of O and Ce overlap. However, the O distribution does not overlap with either Ni or Co. This confirms that Ni and Co co-exist as an alloy, as expected from the phase diagram in Fig. 5 (a). In contrast, after the durability test, oxygen can additionally be found uniformly on the surface of the Ni–Co alloy particles. However, in this case, Co also appears to be more concentrated near the surface of the alloy particles.

Quantitative evaluation of the different ratios of these elements near the surface of the alloy particles was performed using point analysis. Fig. 15(a) shows a STEM image of the $Ni_{95}Co_5$-GDC anode after the redox cycling test, and Fig. 15(b) shows a higher-magnification image of the highlighted area in Fig. 15(a). The ratios of Ni, Co, and O in the $Ni_{95}Co_5$-GDC anode were then compared by point analysis at positions 1, 2, and 3, with 1 being closest to the surface, and 3 being furthest away.

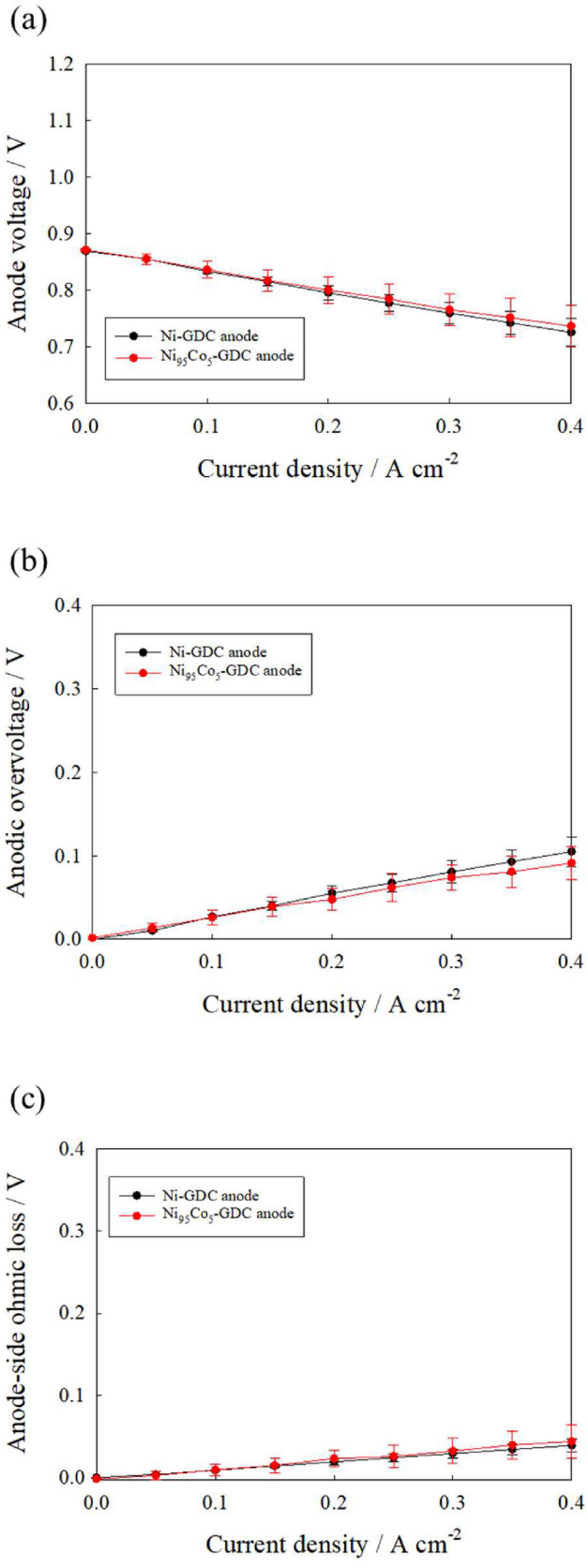

Fig. 10 – Initial electrochemical performance of single cells, for 80% humidified H_2 fuel, using $Ni_{(100-x)}Co_x$-GDC anodes (where x = 0, 5): (a) anode voltage, (b) anodic overvoltage, and (c) anode-side ohmic loss.

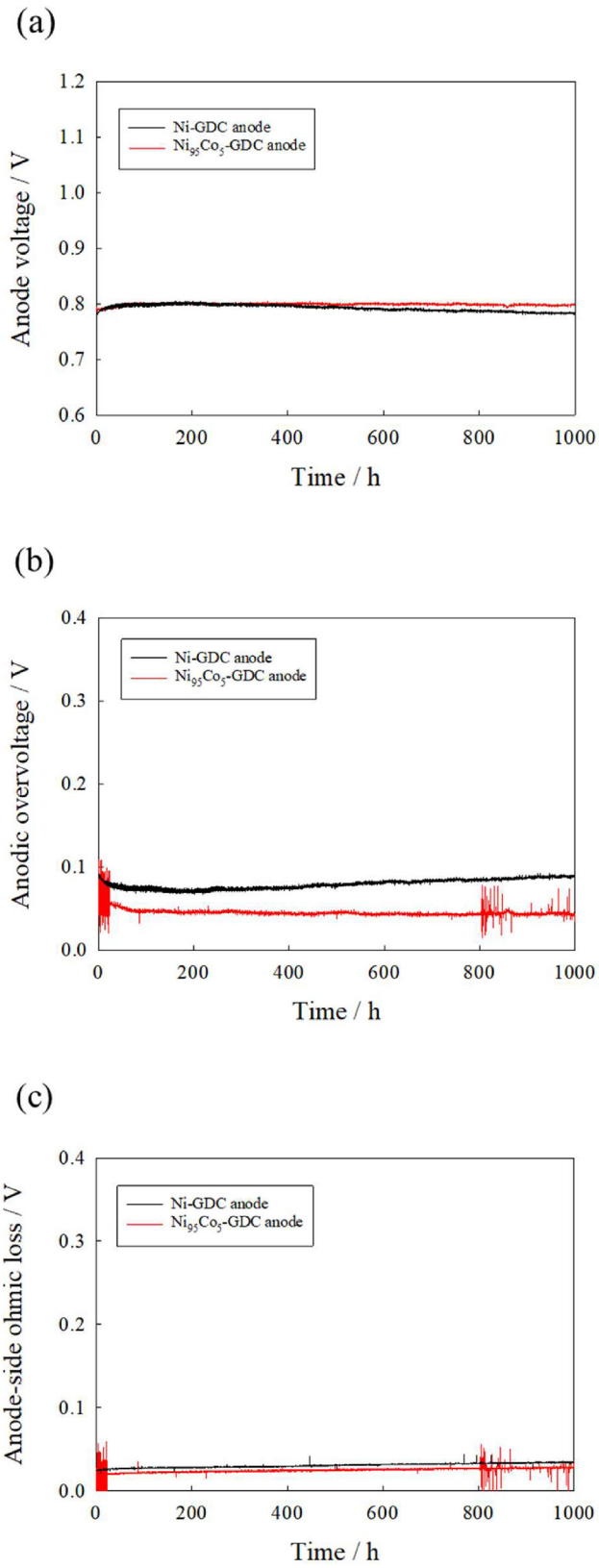

Fig. 11 – Long-term durability up to 1000 h of single cells for 80% humidified H_2 fuel at 0.2 A cm^{-2}, using $Ni_{(100-x)}Co_x$-GDC anode (x = 0, 5): (a) anode voltage, (b) anodic overvoltage, and (c) anode-side ohmic loss.

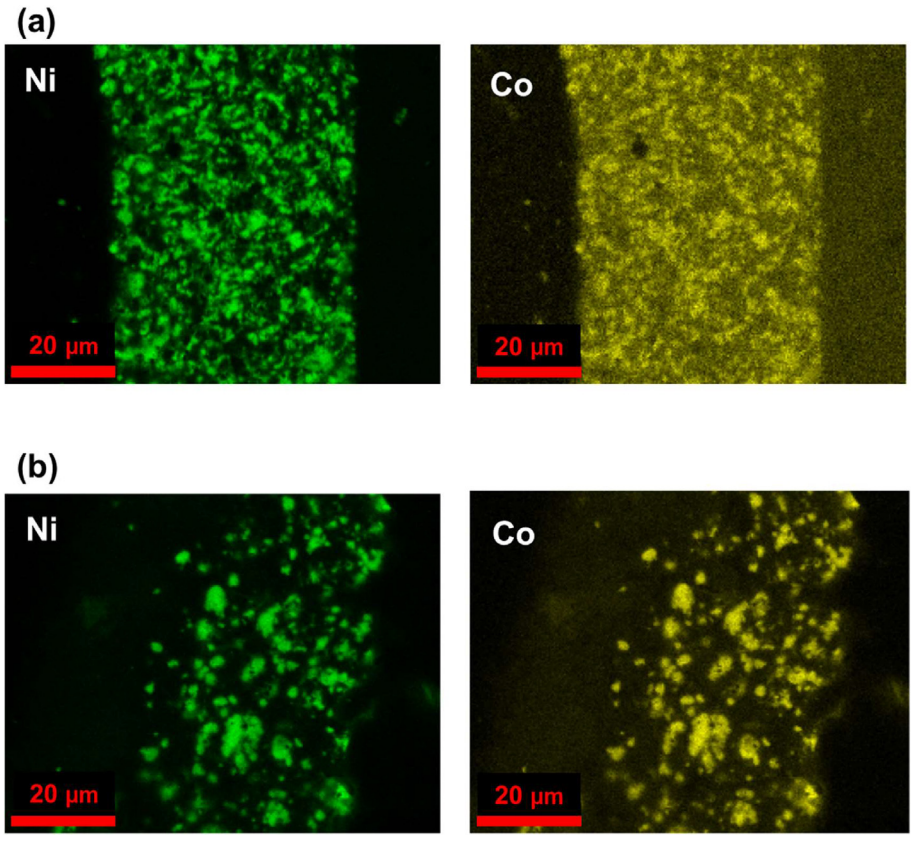

Fig. 12 – Ni and Co mapping images, by EDS analysis, of (a) the $Ni_{95}Co_5$-GDC and (b) the $Ni_{70}Co_{30}$-GDC anodes.

Table 1 – Atomic % of Ni and Co in the $Ni_{95}Co_5$-GDC and $Ni_{70}Co_{30}$-GDC anodes.

	Ni (at. %)	Co (at. %)
$Ni_{95}Co_5$-GDC anode	93.2 ± 0.09	6.8 ± 0.09
$Ni_{70}Co_{30}$-GDC anode	68.9 ± 0.03	31.1 ± 0.03

The particle on the right side of position 1 is GDC. The results of this quantitative analysis are shown in Table 2, confirming that the ratio of O is higher nearer the surface of the alloy particle. Meanwhile, the Ni:Co ratios were 62.6:37.4 at position 1; 91.4:8.6 at position 2; and 92.8:7.2 at position 3, confirming that the Co ratio also increases near the surface. These results clearly indicate that a Co-rich oxide film is formed at the surface of the alloy particles during the redox cycling durability test.

These results confirm that a Ni-based oxide layer is formed on the Ni-GDC anode, while a Co-containing oxide layer is formed on the Ni–Co alloy anode during the redox cycling test. As shown in the stability diagram in Fig. 6, Co is more stable as an oxide than Ni. When NiO is reduced to metallic Ni, aggregation is promoted by the formation of Ni fine particles due to volume shrinkage, as verified by Matsuda et al. [43]. Therefore, when the fuel supply is restarted, the dense oxide layer formed on the Ni–Co alloy anode surface is more stable and more difficult to be reduced compared to the Ni-GDC anode, preventing aggregation during the reduction from NiO to metallic Ni.

The EDS images of the Ni-GDC and $Ni_{95}Co_5$-GDC anodes after 1000-h power generation test under 80% humidified hydrogen supply are shown in Fig. 16. In this case, the Ni-GDC anode images reveal thick oxide layers on the surface of the Ni particles. In contrast, images of the $Ni_{95}Co_5$-GDC anode reveal that both O and Co are present at the surface of Ni–Co alloy particles. These micrographs indicate that a Co-containing dense oxide layer is formed at the surface of the Ni–Co alloy particle even under high water vapor pressure. As mentioned in the previous section, the $Ni_{95}Co_5$-GDC anode suppressed the increase in non-ohmic anodic overvoltage during the 1000-h test under 80% humidified hydrogen supply, compared to the Ni-GDC anode. This can now be directly attributed to the difference in the surface compositions of these two anodes.

Because Ni acts as an excellent catalyst in SOFC anodes, a decrease in the Ni ratio on the particle surface is expected to decrease the electrocatalytic activity. However, in this case the electrode activity is actually maintained in Ni–Co alloys even when the Ni ratio on the electrode surface decreases. In addition, the alloying of the surface may suppress the aggregation of Ni–Co particles. More detailed mechanisms to explain how the high electrocatalytic activity is retained in alloys is of scientific interest in future

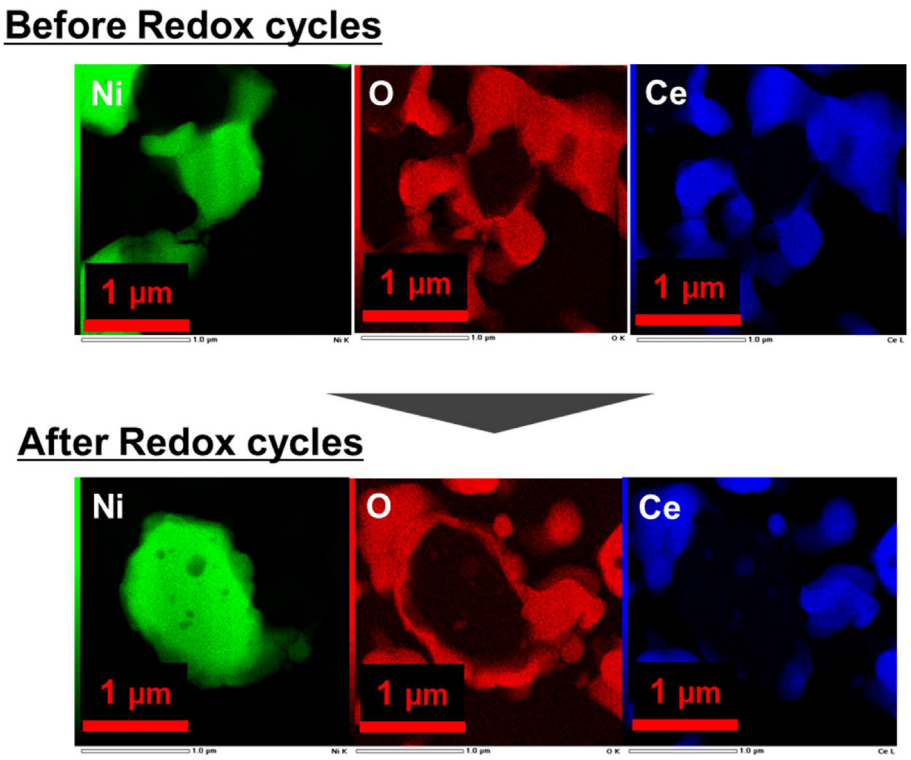

Fig. 13 – Ni, O and Ce mapping, by EDS analysis, of the Ni-GDC anode before and after the redox cycle durability tests.

studies, and further investigation is needed. This will be performed via e.g. quantitative particle size analysis, impedance measurements, and distribution of relaxation time (DRT) analysis.

When these alternative anode materials are applied to practical SOFCs, it will also be essential to evaluate the effects of using impurity-containing fuels [44–51]. Sulfur is a typical SOFC fuel impurity causing cell voltage drop [44–46]. Chlorine

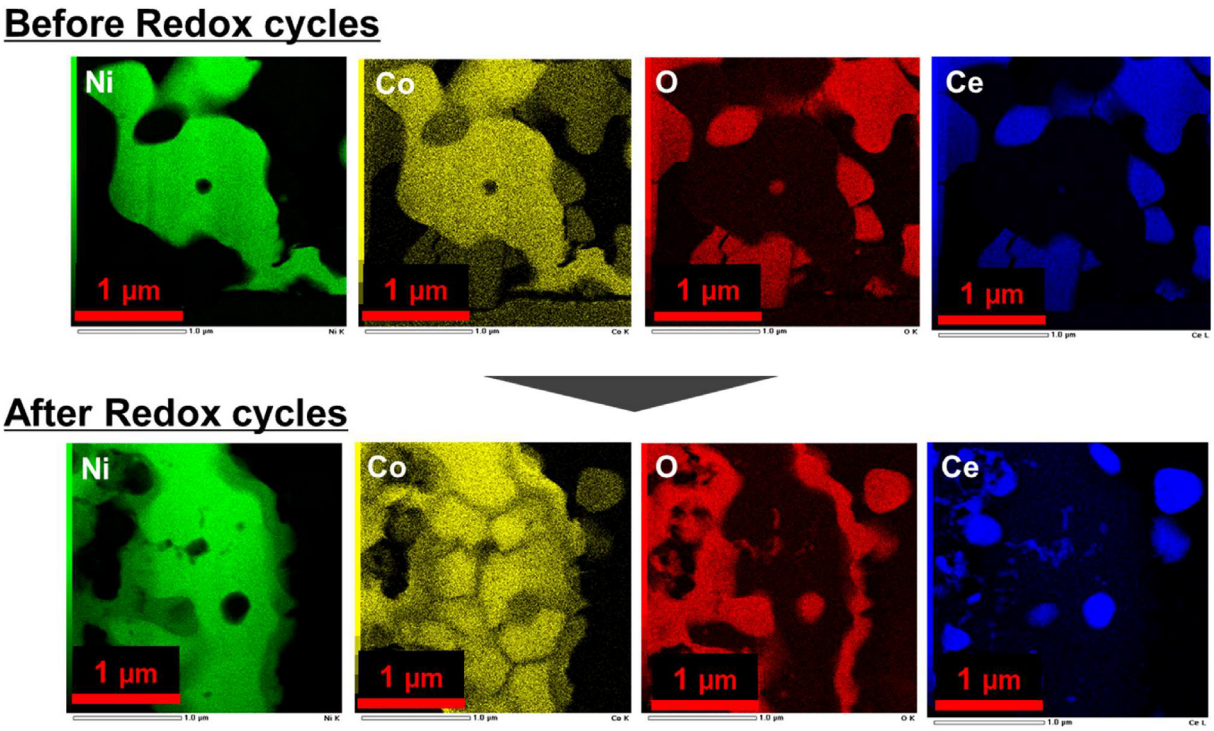

Fig. 14 – Ni, Co, O and Ce mapping, by EDS analysis, of the $Ni_{95}Co_5$-GDC anode before and after the redox cycle durability tests.

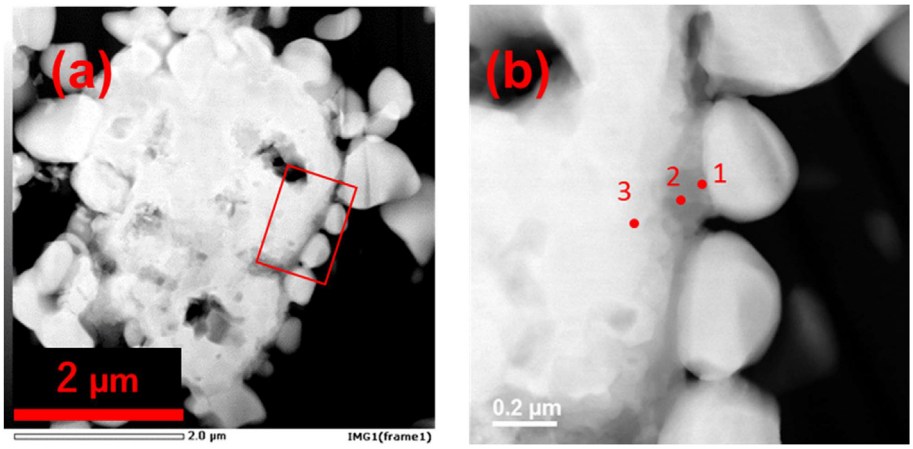

Fig. 15 – (a) STEM image of the $Ni_{95}Co_5$-GDC anode after redox cycle durability tests; and (b) a higher-magnification image of the area enclosed by the red box in (a). (For interpretation of the references to color in this figure legend, the reader is referred to the Web version of this article.)

Table 2 – Atomic % of Ni, Co, and O at three positions, 1, 2 and 3 in a Ni–Co alloy particle shown in Fig. 15 (b).

	Ni (at. %)	Co (at. %)	O (at. %)
Position No. 1	35.2	21.0	43.8
Position No. 2	59.6	5.6	34.8
Position No. 3	83.9	6.5	9.6

is another typical trace impurity in e.g. tap water [44,45,47], while phosphorous causes serious degradation even at ppb levels [44,45]. Siloxane is a contaminant in e.g. digester gas causing silica formation [44,45]. Trace impurities in biofuels affect the performance and durability of SOFCs [48–51]. As such, it will be important to evaluate impurity poisoning in Ni–Co alloy anodes in future studies, associated with various chemical reactions with Ni and/or Co.

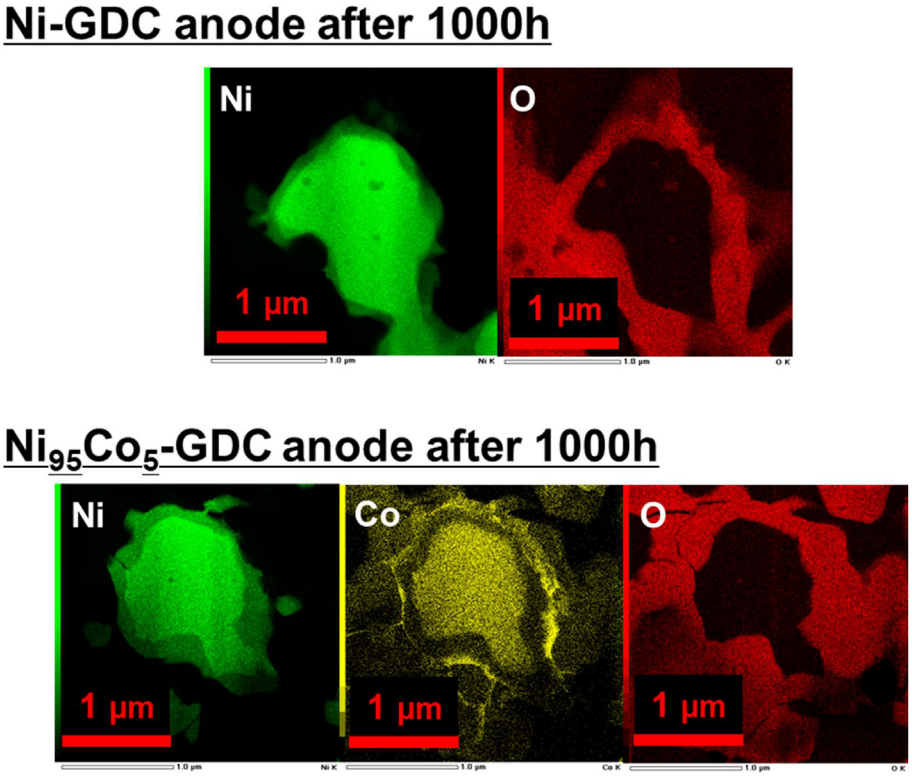

Fig. 16 – Ni, Co and O mapping, by EDS analysis, of the Ni-GDC and $Ni_{95}Co_5$-GDC anodes after the 1000h durability test for 80% humidified H_2 fuel, at 0.2 A cm^{-2}.

Conclusions

Ni–Co alloy cermet anodes for SOFCs were prepared and compared to pure-Ni cermet anodes. The initial I–V performance of the Ni–Co alloy anodes was comparable to that of the Ni-based anode. The redox cycling durability was considerably improved by alloying, even at low concentrations of 5 mol%. A 1000-h durability test was performed using highly humidified hydrogen supply, confirming that alloying can suppress increases in non-ohmic anodic overvoltage without compromising the I–V performance, even at high fuel utilization. Electron microscopy revealed that for pure Ni-based anodes, a nickel oxide layer is formed on the surface of the Ni particles, while in the case of alloy anodes, a Co-containing oxide layer is formed during operation. Since Co is a more stable oxide compared to Ni, this Co-containing oxide layer suppresses aggregation of Ni-based particles under redox cycling, or at high water vapor partial pressure. As such, Ni–Co alloy can be regarded as a robust cermet anode material for SOFCs, realizing high electrochemical performance, redox cycling durability, and long-term durability even under a high water vapor atmosphere, and with a Co content as low as 5 mol%. As such redox-stability is more critical for anode-supported cells than for electrolyte-supported cells, it is of technological interest to apply the redox-stable alloy anode material to anode-supported SOFCs and related electrochemical cells.

Declaration of competing interest

The authors declare that they have no known competing financial interests or personal relationships that could have appeared to influence the work reported in this paper.

Acknowledgements

A part of this study was supported by "Research and Development Program for Promoting Innovative Clean Energy Technologies Through International Collaboration" of the New Energy and Industrial Technology Development Organization (NEDO) (Project No. JPNP20005). Collaborative support by Prof. H. L. Tuller, Prof. B. Yildiz, and Prof. J. L. M. Rupp at Massachusetts Institute of Technology (MIT) is gratefully acknowledged.

Nomenclature

Abbreviations

DRT	distribution of relaxation time
EDS	energy-dispersive X-ray spectroscopy
GDC	gadolinium-doped ceria
LSM	lanthanum strontium manganite
LST	lanthanum-doped strontium titanate
ScSZ	scandium-stabilized zirconia
SEM	scanning electron microscopy
SOFC	solid oxide fuel cell
STEM	scanning transmission electron microscopy

REFERENCES

[1] Minh NQ. Ceramic fuel cells. J Am Ceram Soc 1993;76(3):563–88. https://doi.org/10.1111/j.1151-2916.1993.tb03645.x.
[2] Brandon NP, Skinner S, Steele BCH. Recent advances in materials for fuel cells. Annu Rev Mater Res 2003;33(1):183–213. https://doi.org/10.1146/annurev.matsci.33.022802.094122.
[3] Singhal SC, Kendall K. High temperature solid oxide fuel cells: fundamentals, design, and applications. Elsevier; 2003.
[4] Vielstich W, Lamm A, Gasteiger A, editors. Handbook of fuel cells: fundamentals, Technology and applications. John Wiley & Sons Ltd; 2003.
[5] Mench MM. Fuel cell engines. John Wiley & Sons, Inc.; 2008.
[6] Sasaki K, Li HW, Hayashi A, Yamabe J, Ogura T, Lyth SM, editors. Hydrogen energy engineering: a Japanese perspective. Springer Japan; 2016.
[7] ENEFARM PARTNERS homepage [in Japanese], https://www.gas.or.jp/user/comfortable-life/enefarm-partners/.
[8] Ministry of Economy. Trade and industry (Japan), hydrogen and fuel cell strategic roadmap [in Japanese], https://www.nedo.go.jp/content/100895058.pdf.
[9] Kobayashi Y, Tomida K, Nishiura M, Hiwatashi K, Kishizawa H, Takenobu K. Development of next-generation large-scale SOFC toward realization of a Hydrogen Society. Mitsubishi Heavy Ind Tech Rev 2015;52(2):6.
[10] Leah R, Bone A, Selcuk A, Lankin M, Rahman M, Clare A, Reade G, Felix F, De Vero J, Wang Xi, Mukerjee S, Selby M. Commercialization of the Ceres power SteelCell ® Technology: latest update. ECS Trans 2021;103(1):679–84. https://doi.org/10.1149/10301.0679ecst.
[11] Mendonça C, Ferreira A, Santos DMF. Towards the commercialization of solid oxide fuel cells: recent advances in materials and integration strategies. Fuel 2021;2(4):393–419. https://doi.org/10.3390/fuels2040023.
[12] Patakangas J, Ma Y, Jing Y, Lund P. Review and analysis of characterization methods and ionic conductivities for low-temperature solid oxide fuel cells (LT-SOFC). J Power Sources 2014;263:315–31. https://doi.org/10.1016/j.jpowsour.2014.04.008.
[13] Fu CJ, Chan SH, Ge XM, Liu QL, Pasciak G. A promising Ni–Fe bimetallic anode for intermediate-temperature SOFC based on Gd-doped ceria electrolyte. Int J Hydrogen Energy 2011;36(21):13727–34. https://doi.org/10.1016/j.ijhydene.2011.07.119.
[14] Yu JH, Park GW, Lee S, Woo SK. Microstructural effects on the electrical and mechanical properties of Ni–YSZ cermet for SOFC anode. J Power Sources 2007;163(2):926–32. https://doi.org/10.1016/j.jpowsour.2006.10.017.
[15] Hanasaki M, Uryu C, Daio T, Kawabata T, Tachikawa Y, Lyth SM, Shiratori Y, Taniguchi S, Sasaki K. SOFC durability against standby and shutdown cycling. J Electrochem Soc 2014;161(9):F850–60. https://doi.org/10.1149/2.0421409jes.
[16] Waldbillig D, Wood A, Ivey D. Thermal analysis of the cyclic reduction and oxidation behaviour of SOFC anodes. Solid State Ionics 2005;176(9–10):847–59. https://doi.org/10.1016/j.ssi.2004.12.002.
[17] Dikwal CM, Bujalski W, Kendall K. Characterization of the electrochemical performance of micro-tubular SOFC in partial reduction and oxidation conditions. J Power Sources

2008;181(2):267–73. https://doi.org/10.1016/j.jpowsour.2007.11.052.
[18] Guan Y, Gong Y, Li W, Gelb J, Zhang L, Liu G, Zhang X, Song X, Xia C, Xiong Y, Wang H, Wu Z, Tian Y. Quantitative analysis of micro structural and conductivity evolution of Ni-YSZ anodes during thermal cycling based on nano-computed tomography. J Power Sources 2011;196(24):10601–5. https://doi.org/10.1016/j.jpowsour.2011.08.083.
[19] Iwata T. Characterization of Ni-YSZ anode degradation for substrate-type solid oxide fuel cells. J Electrochem Soc 1996;143(5):1521–5. https://doi.org/10.1149/1.1836673.
[20] Itoh H, Yamamoto T, Mori M, Horita T, Sakai N, Yokokawa H, Dokiya M. Configurational and electrical behavior of Ni-YSZ cermet with novel microstructure for solid oxide fuel cell anodes. J Electrochem Soc 1997;144(2):641–6. https://doi.org/10.1149/1.1837460.
[21] Kawasaki T, Sugimoto J, Tachikawa Y, Shiratori Y, Taniguchi S, Sasaki K. Oxidation-induced degradation of SOFC Ni anodes at high fuel utilizations. ECS Trans 2015;68(1):1345–52. https://doi.org/10.1149/06801.1345ecst.
[22] Malzbender J, Wessel E, Steinbrech R. Reduction and Re-oxidation of anodes for solid oxide fuel cells. Solid State Ionics 2005;176(29–30):2201–3. https://doi.org/10.1016/j.ssi.2005.06.014.
[23] Fujita K, Somekawa T, Hatae T, Matsuzaki Y. Residual stress and redox cycling of segmented-in-series solid oxide fuel cells. J Power Sources 2011;196(21):9022–6. https://doi.org/10.1016/j.jpowsour.2011.01.022.
[24] Kubota M, Okanishi T, Muroyama H, Matsui T, Eguchi K. Microstructural evolution of Ni–YSZ cermet anode under thermal cycles with redox treatments. J Electrochem Soc 2015;162(4):F380–6. https://doi.org/10.1149/2.0311504jes.
[25] Sumi H, Kishida R, Kim J-Y, Muroyama H, Matsui T, Eguchi K. Correlation between microstructural and electrochemical characteristics during redox cycles for Ni–YSZ anode of SOFCs. J Electrochem Soc 2010;157(12):B1747. https://doi.org/10.1149/1.3491345.
[26] Fang Q, Blum L, Peters R, Peksen M, Batfalsky P, Stolten D. SOFC stack performance under high fuel utilization. Int J Hydrogen Energy 2015;40(2):1128–36. https://doi.org/10.1016/j.ijhydene.2014.11.094.
[27] Shen X, Sasaki K. Highly redox-resistant solid oxide fuel cell anode materials based on La-doped $SrTiO_3$ by catalyst impregnation strategy. J Power Sources 2016;320:180–7. https://doi.org/10.1016/j.jpowsour.2016.04.111.
[28] Shen X, Sasaki K. Robust SOFC anode materials with La-doped $SrTiO_3$ backbone structure. Int J Hydrogen Energy 2016;41(38):17044–52. https://doi.org/10.1016/j.ijhydene.2016.08.024.
[29] Futamura S, Tachikawa Y, Matsuda J, Lyth SM, Shiratori Y, Taniguchi S, Sasaki K. Alternative Ni-impregnated mixed ionic-electronic conducting anode for SOFC operation at high fuel utilization. J Electrochem Soc 2017;164(10):F3055–63. https://doi.org/10.1149/2.0071710jes.
[30] Futamura S, Muramoto A, Tachikawa Y, Matsuda J, Lyth SM, Shiratori Y, Taniguchi S, Sasaki K. SOFC anodes impregnated with noble metal catalyst nanoparticles for high fuel utilization. Int J Hydrogen Energy 2019;44(16):8502–18. https://doi.org/10.1016/j.ijhydene.2019.01.223.
[31] Wang Z, Mori M. Sintering characteristics and electrical conductivity of $(Sr_{1-x}La_x)TiO_3$ synthesized by the citric acid method. J Fuel Cell Sci Technol 2011;8(5):51018. https://doi.org/10.1115/1.4003993.
[32] Marina O. Thermal, electrical, and electrocatalytical properties of lanthanum-doped strontium titanate. Solid State Ionics 2002;149(1–2):21–8. https://doi.org/10.1016/S0167-2738(02)00140-6.
[33] Sun X, Wang S, Wang Z, Ye X, Wen T, Huang F. Anode performance of LST–xCeO_2 for solid oxide fuel cells. J Power Sources 2008;183(1):114–7. https://doi.org/10.1016/j.jpowsour.2008.05.007.
[34] Yoo KB, Choi GM. LST–GDC composite anode on $LaGaO_3$-based solid oxide fuel cell. Solid State Ionics 2011;192(1):515–8. https://doi.org/10.1016/j.ssi.2010.06.048.
[35] Chen G, Kishimoto H, Yamaji K, Kuramoto K, Horita T. Effect of interaction between A-site deficient LST and ScSZ on electrochemical performance of SOFC. J Electrochem Soc 2015;162(3):F223–8. https://doi.org/10.1149/2.0131503jes.
[36] Kittel C. Introduction to solid state physics. 8th ed. New York: Wiley; 2004.
[37] Araki K, Yamamoto J, Shiratori Y, Ito K, Sasaki K. Performance and long-term durability of nanostructured Ni anodes doped with transition metals prepared by spray mist dryer. ECS Trans 2019;25(2):2039–48. https://doi.org/10.1149/1.3205749.
[38] Ishibashi Y, Matsumoto K, Futamura S, Tachikawa Y, Matsuda J, Lyth SM, Shiratori Y, Taniguchi S, Sasaki K. Improved redox cycling durability in alternative Ni alloy-based SOFC anodes. J Electrochem Soc 2020;167(12):124517. https://doi.org/10.1149/1945-7111/abac87.
[39] David M, Lyth SM, Lindner R, Harrington GF. Future-proofing fuel cells, critical raw material governance in sustainable energy. Palgrave Macmillan; 2021.
[40] Jha MK, Kumari A, Jha AK, Kumar V, Hait J, Pandey BD. Recovery of lithium and cobalt from waste lithium ion batteries of mobile phone. Waste Manag 2013;33(9):1890–7. https://doi.org/10.1016/j.wasman.2013.05.008.
[41] Li M, Lu J. Cobalt in lithium-ion batteries. Science 2020;367(6481):979–80. https://doi.org/10.1126/science.aba9168.
[42] Matsui T, Kishida R, Kim J-Y, Muroyama H, Eguchi K. Performance deterioration of Ni–YSZ anode induced by electrochemically generated steam in solid oxide fuel cells. J Electrochem Soc 2010;157(5):B776. https://doi.org/10.1149/1.3336830.
[43] Matsuda J, Kawasaki T, Futamura S, Kawabata T, Taniguchi S, Sasaki K. *In* situ transmission electron microscopic observations of redox cycling of a Ni–ScSZ cermet fuel cell anode. Microscopy 2018;67(5):251–8. https://doi.org/10.1093/jmicro/dfy025.
[44] Matsuda J, Kawasaki T, Futamura S, Kawabata T, Taniguchi S, Sasaki K. *In* situ transmission electron microscopic observations of redox cycling of a Ni–ScSZ cermet fuel cell anode. Microscopy 2018;67(5):251. https://doi.org/10.1093/jmicro/dfy025.
[45] Haga K, Adachi S, Shiratori Y, Itoh K, Sasaki K. Poisoning of SOFC anodes by various fuel impurities. Solid State Ionics 2008;179(27–32):1427–31. https://doi.org/10.1016/j.ssi.2008.02.062.
[46] Haga K, Shiratori Y, Ito K, Sasaki K. Chlorine poisoning of SOFC Ni-cermet anodes. J Electrochem Soc 2008;155(12):B1233–9. https://doi.org/10.1149/1.2980521.
[47] Haga K, Shiraton Y, Nojiri Y, Ito K, Sasaki K. Phosphorus poisoning of Ni-cermet anodes in solid oxide fuel cells. J Electrochem Soc 2010;157(11):1693–700. https://doi.org/10.1149/1.3489265.
[48] Lanzini A, Madi H, Chiodo V, Papurello D, Maisano S, Santarelli M, Van herle J. Dealing with fuel contaminants in biogas-fed solid oxide fuel cell (SOFC) and molten carbonate fuel cell (MCFC) plants: degradation of catalytic and electro-catalytic active surfaces and related gas purification methods. Prog Energy Combust Sci 2017;61:150–88. https://doi.org/10.1016/j.pecs.2017.04.002.
[49] Papurello D, Silvestri S, Modena S. Biogas trace compounds impact on high-temperature fuel cells short stack

performance. Int J Hydrogen Energy 2021;46(12):8792–801. https://doi.org/10.1016/j.ijhydene.2020.11.273.

[50] Papurello D, Canuto D, Santarelli M. CFD model for tubular SOFC stack fed directly by biomass. Int J Hydrogen Energy 2022;47(10):6860–72. https://doi.org/10.1016/j.ijhydene.2021.12.015.

[51] Panagi K, Laycock CJ, Reed JP, Alan J, Guwy AJ. The effects of fuel variability on the electrical performance and durability of a solid oxide fuel cell operating on biohythane. Int J Hydrogen Energy 2021;46(2):2630–45. https://doi.org/10.1016/j.ijhydene.2020.10.151.